Proceedings of the International Gas Turbine Congress 2003 Tokyo
November 2-7, 2003

IGTC2003 Tokyo TS-034

New Quasi-3D Inverse Navier-Stokes Based Method Used to Design Highly Loaded Axial Compressor Stages

Victor I. MILESHIN, Sergey K. SHCHIPIN and Andrew N. STARTSEV

Central Institute of Aviation Motors
2, Aviamotornaya St., 111116, Moscow, RUSSIA
Phone: +007 (095) 362-2194, Fax: +007 (095) 361-6696, E-mail address: mileshin@ciam.ru

ABSTRACT

Present paper contains a method of solution of inverse problem for Navier-Stokes equations for quasi-3D flows without any simplification of the problem statement and applied to design of turbomachinery bladed rows.

In the developed method blade surface is impermeable and no-slip or any other boundary condition compatible with Navier-Stokes equations is applied on the blade surface. Solution of inverse problem is determined using moving grid, which is re-generated at each step of time-marching procedure (variation of flow-rate, impulse and energy fluxes due to movement of grid nodes is taken into account). Normal speed of face of grid cell adjacent to blade surface is determined using given static pressure (inverse mode) with the aid of relationships which are the elements of Godunov scheme applied for integration of flow equations.

INTRODUCTION

During last two decades a number of emerging 2D Euler-based inverse design methods have been developed (Meauze, G., 1982, and Demeulenaere, A., et al., 1997). However only a few of them can be generalized for 3D inverse design. Thus any new method of solution of 3D inverse problem even for Euler equations is an important achievement (Dang, T., et al., 2000).

The most ambitious problem is solution of 3D inverse problem for Navier-Stokes equations. Up to now no rigorous solution of inverse problem for Navier-Stokes equations exists even for 2D problem. Known methods of solution of inverse problem for Navier-Stokes equations consist in combination of direct mode (analysis) for Navier-Stokes equations (de Vito, L., et al., 2002) and inverse mode (design) for Euler equations. Another approach to solve inverse problem for Navier-Stokes equations consists in application of model of permeable wall (Demeulenaere, A., et al., 1997). Here, it is worth noting that model of permeable wall based on flow-rate conservation requires non-zero tangential velocity at the wall, whereas this velocity for viscous flow has to be zero. Besides that, method (Demeulenaere, A., et al., 1997) demonstrates serious problems with convergence in case of transonic flows.

Mentioned combination of direct mode (analysis) for Navier-Stokes equations (de Vito, L., et al., 2002) and inverse mode (design) for Euler equations is of limited application in case of presence of viscous flow separation zone at the blade surface, because in the case blade surface pressure depends on the shape of separation zone instead of blade geometry.

Present paper contains method of solution of inverse problem for Navier-Stokes equations for quasi-3D flows, which is free of drawbacks mentioned above.

Method is based on V. Mileshin's algorithm of solution of quasi-3D inverse problem for Euler equations developed in 1990 (Mileshin, V.I., 1992 and Mileshin, V.I., 2000). This algorithm can be extended to 3D Euler equations. More valuable feature is its applicability to quasi-3D and 3D Navier-Stokes equations without any simplification of the problem statement.

In the developed method blade surface is impermeable and no-slip or any other boundary condition compatible with Navier-Stokes equations is applied on the blade surface. Solution of inverse problem is determined using moving grid, which is re-generated at each step of time-marching procedure (variation of flow-rate, impulse and energy fluxes due to movement of grid nodes is taken into account). Normal speed of face of grid cell adjacent to blade surface is determined using given static pressure (inverse mode) with the aid of relationships which are the elements of Godunov scheme applied for integration of flow equations. Cell face adjacent to blade surface is impermeable during the movement process. Location of grid nodes adjacent to blade surface is determined at each new step of time-marching procedure using special algorithm maintaining self-stabilization of new blade surface, i.e. preventing kinks, saw and so on.

It is important to note that analysis (direct mode) of quasi-3D viscous flows uses the same solution algorithm as that of inverse mode solution for quasi-3D problem statements correspondingly.

GOVERNING EQUATIONS FOR QUASI-3D INVERSE METHOD AND ELEMENTS OF NUMERICAL SCHEME

Quasi-3D flow analysis of bladed cascades on the non-cylindrical surface of revolution uses the following coordinate system: **m** the meridional curvilinear abscissa, θ the circumferential coordinate. The coordinates **m** and θ are determined from cylindrical coordinates according to the formulae:

$$dm^2 = dz^2 + dr^2 \qquad (1)$$

$$\theta = \theta' - \Omega t \qquad (2)$$

Here the angle θ' is measured in fixed coordinate system, and θ - in rotating relative coordinate system turning with bladed row with the angular velocity $\boldsymbol{\Omega}$. Radius **r** and variable stream tube thickness **b** are taken as given functions of **m**. In chosen coordinate system non-dimensional Navier-Stokes equations can be written in a near-conservative form:

$$\partial_t \vec{q} + \partial_m (\vec{F} - \mathrm{Re}^{-1} \cdot \vec{R}) + \partial_\theta (\vec{G} - \mathrm{Re}^{-1} \vec{S}) = \vec{K} \qquad (3)$$

Manuscript Received on July 4, 2003

Here

$$\vec{q} = rb\begin{bmatrix}\rho\\ \rho\cdot w_m\\ \rho\cdot w_\theta\\ \rho\cdot J - p\end{bmatrix};\ \vec{F} = rb\begin{bmatrix}\rho\cdot w_m\\ p+\rho\cdot w_m^2\\ \rho\cdot w_\theta w_m\\ \rho\cdot J w_m\end{bmatrix};$$

$$\vec{G} = b\begin{bmatrix}\rho\cdot w_\theta\\ \rho\cdot w_m w_\theta\\ p+\rho\cdot w_\theta^2\\ \rho\cdot J w_\theta\end{bmatrix};\qquad \vec{K} = \begin{bmatrix}0\\ K_2\\ K_3\\ 0\end{bmatrix};\qquad (4)$$

$$K_2 = p\frac{d(br)}{dm} + \rho\cdot b(w_\theta+\Omega r)^2\frac{dr}{dm} - \mathrm{Re}^{-1}(\sigma_{22}b\frac{dr}{dm} + \sigma_{33}r\frac{db}{dm});$$

$$K_3 = b\left[\mathrm{Re}^{-1}\sigma_{12} - \rho\cdot w_m(w_\theta+2\Omega r)\right]\frac{dr}{dm};$$

$$\vec{R} = rb\begin{bmatrix}0\\ \sigma_{11}\\ \sigma_{12}\\ R_4-\Omega r\sigma_{12})\end{bmatrix};\quad \vec{S} = b\begin{bmatrix}0\\ \sigma_{12}\\ \sigma_{22}\\ (S_4-\Omega r\sigma_{22})\end{bmatrix};$$

Here $\boldsymbol{p}$ is the pressure; $\boldsymbol{\rho}$ the density; $\boldsymbol{w_m}$ and $\boldsymbol{w_\theta}$ are the relative velocity components $\vec{\mathbf{W}}$;

$\mathrm{J} = \varepsilon + \frac{\mathrm{p}}{\rho} + \frac{1}{2}(\mathrm{w}_\mathrm{m}^2 + \mathrm{w}_\theta^2) - \frac{\Omega^2\mathrm{r}^2}{2}$ is the rothalpy;

$\varepsilon = \frac{1}{æ - 1}\cdot\frac{\mathrm{p}}{\rho}$ is the internal energy per unit mass of fluid.

Terms of energy equation standing for viscous transfer are as follows:

$$R_4 = \frac{k}{(æ-1)\,\mathrm{Pr}}\left[\partial_m a^2 + w_m\sigma_{11} + (w_\theta+\Omega r)\sigma_{12}\right] \quad (5)$$

$$S_4 = \frac{k}{(æ-1)\,\mathrm{Pr}}\left[\frac{\partial a^2}{r} + w_m\sigma_{12} + (w_\theta+\Omega r)\sigma_{22}\right];$$

Here **æ** is the ratio of specific heats; $\mathrm{a} = \sqrt{\frac{æ\mathrm{p}}{\rho}}$ the speed of sound, and the corrected thermal conductivity ***k*=1.**

Components of tensor of viscous stresses are calculated from the formulae:

$$\sigma_{11} = 2\mu\cdot\partial_m w_m + \lambda\cdot\nabla\vec{W};$$

$$\sigma_{22} = 2\mu\cdot(\partial_\theta w_\theta + w_m\frac{dr}{dm})/r + \lambda\cdot\nabla\vec{W};$$

$$\sigma_{33} = 2\mu\cdot w_m\frac{1}{b}\frac{db}{dm} + \lambda\cdot\nabla\vec{W}; \quad (6)$$

$$\sigma_{12} = \mu\cdot(\partial_m w_\theta - \frac{w_\theta}{r}\frac{dr}{dm} + \frac{1}{r}\partial_\theta w_m);$$

$$\lambda\cdot\nabla\cdot\vec{W} = -\frac{2}{3}\mu\cdot\left[\partial_m w_m + w_m(\frac{1}{r}\frac{dr}{dm} + \frac{1}{b}\frac{db}{dm}) + \frac{\partial_\theta w_\theta}{r}\right];$$

We use stagnation density of the entering gas and critical speed of sound in relative motion to bring the Eq.1÷6 into the non-dimensional form.

To outline turbulent flows, Baldwin-Lomax two-layer algebraic eddy viscosity model is applied (Baldwin, B.W., 1978).

For integration of Eq.1-6 we use modified scheme by S.K. Godunov (Mileshin, V.I., et al., 2000, and Ivanov, M.Ya., et al., 1989, and Kopchenov, V.I., et al., 1994). According to the modified scheme of S.K.Godunov, non-stationary Navier –Stokes equations are written as integral conservation laws for a volume of space and an interval of time taking into account grid velocity due to motion of the volume's faces along the stream-surface ***(m, θ)***.

$$\frac{d}{dt}\iint_{A(t)}\vec{q}\,dm\,d\theta + \oint_{L(t)}\left[(\vec{F} - \mathrm{Re}^{-1}\vec{R} - \vec{q}D_m)d\theta - (\vec{G} - \mathrm{Re}^{-1}\cdot\vec{S} - \vec{q}D_\theta)dm\right] = \iint_{A(t)}\vec{K}\,dm\,d\theta \quad (7)$$

Here ***A(t)*** is the ***(m, θ)*** stream-surface's element arbitrarily varying in time**;** ***L(t)*** its boundary; $\boldsymbol{D_m}$ and $\boldsymbol{D_\theta}$ are the components of the boundary velocity which is normal to the boundary ***L(t)*** and tangential to the stream-surface ***(m, θ).***

Time-marching procedure generates stationary flow beginning with fairly arbitrary initial and boundary conditions. Time-marching procedure is developed for moving grid. Grid motion is computed from a change of the airfoil's shape determined at each time step.

Explicit Godunov scheme of raised order of accuracy (Mileshin, V.I., 1992), or implicit modified Godunov scheme (Kopchenov, V.I., et al., 1994) are used to integrate the set of Eq.7.

BOUNDARY CONDITIONS

Flow functions have to comply with given flow conditions on the boundaries of computational domain. Type and number of the boundary conditions are obtained in accord with principles set out in (Mileshin, V.I., et al., 2000, and Godunov, S.K., et al., 1976, and Ivanov, M.Ya., et al., 1989).

For subsonic entering flow, total pressure, stagnation temperature and flow angle are specified at inlet. At periodic boundary, the missing values at points outside the computational domain are replaced by the values at corresponding points at the other periodic boundary. Along the airfoil surface, boundary condition depends on the mode of computation: in case of direct mode boundary condition imposes the slope of the velocity vector, in case of inverse mode pressure distribution along the airfoil surface is imposed. Given pressure is used as a boundary condition at outlet.

Applying inverse mode, in advance it is difficult to guess correct pressure distribution providing trailing edge closure and avoiding self-intersection of airfoil contour. To eliminate this difficulty pressure distribution is on either suction or pressure side of the airfoil. The other side is

defined from the condition of given airfoil thickness distribution.

GRID GENERATION

To simplify implementation of the inverse method, we use the curvilinear H-type grid with exponential stretching of grid nodes to airfoil's leading and trailing edges and to its surfaces. Grid is analytically tractable saving CPU time for its generation at each time step (Fig.1).

ALGORITHM OF THE AIRFOIL DESIGN

As is done in Godunov scheme (Godunov, S.K., et al., 1976), exact Riemann solver is applied to obtain numerical fluxes over each face of a cell using known flow parameters in the centers of neighboring cells. In particular, normal to the airfoil surface component of velocity $\vec{\mathbf{D}}$ is obtained from known parameters in cells neighboring airfoil surface and from given pressure distribution along the surface noting that locally airfoil contour matches with contact discontinuity. Thus the problem of geometrical construction of the airfoil surface reduces to the resolution of contact discontinuity precisely computed by exact Riemann solver. Solution of Riemann problem is used for airfoil construction both in case of Euler equations and Navier-Stokes equations. Only in case of Navier-Stokes equations we use modified Godunov's scheme (Mileshin, V.I., et al., 2000, and Godunov, S.K., et al., 1976, and Kopchenov, V.I., et al., 1994).

Also notice that there is no leakage through the contact discontinuity, i.e. at each time step $(t+\tau)$ the flow direction is parallel to the moving airfoil surface. Velocity of contact discontinuity determines displacement of the airfoil surface. For example, the component of velocity of suction surface displacement in the direction normal to the surface, for the cascade shown on Fig.1, is calculated from the Eq.10:

$$D_{ss} = \frac{(PP_{ss} - p_{ss})}{A0}, \quad (8)$$

and velocity of pressure surface displacement is obtained from the formula:

$$D_{ps} = -\frac{(PP_{ps} - p_{ps})}{A0}, \quad (9)$$

here $\mathbf{PP_{ss}}$ and $\mathbf{PP_{ps}}$ are given pressures on suction and pressure surfaces correspondingly, $\mathbf{p_{ss}}$ and $\mathbf{p_{ps}}$ are pressures in cells neighboring airfoil surface, $\mathbf{A0}$ is the mass velocity Eq.10.

The value of $\mathbf{A0}$ is determined from the following formula Eq.10:

if $PP_{SS} \geq p_{SS,}$ then

$$A0 = \sqrt{(\frac{æ+1}{2} \cdot PP_{SS} + \frac{æ-1}{2} p_{SS})\rho_{SS}}; \quad (10)$$

if $PP_{SS} < p_{SS,}$ then

$$A0 = \frac{æ-1}{2æ} \rho_{SS} a_{SS} \frac{1 - \frac{PP_{SS}}{p_{SS}}}{1 - (\frac{PP_{SS}}{p_{SS}})^{\frac{æ-1}{2æ}}}; \quad (11)$$

Obtained normal velocities of the airfoil surface segments movement $\mathbf{D_{ss}}$ or $\mathbf{D_{ps}}$ determine the surface normal displacement $\Delta = \tau \cdot \mathbf{D}$ in a time step τ. Because grid at the moment $(t+\tau)$ is determined by new location of nodes along the guidelines of the grid, then its construction consists in calculation of the nodes displacement, not the surface segments displacements. Fig.1 demonstrates computation grid and domain. Vertical grid lines are fixed and used as guidelines; grid lines crossing them are movable.

Calculation of normal surface velocities is important for geometrical construction of airfoil, but it is not enough for successful construction. It is due to fairly arbitrary initial values of flow parameters in grid cells generating shock waves on airfoil surface or other flow singularities, which cause steep gradients of flow parameters. Non-uniformity of flow parameters may cause saw-like surface of airfoil and instability of the inverse problem solution.

To eliminate such instability, geometrical construction of the airfoil has to stabilize itself. Geometrical construction algorithm has to provide restricted velocity of node displacement along the guideline even in case of saw-like airfoil surface. For the saw-like airfoil, node velocity is remarkably larger than normal surface velocity.

To restrict this velocity let use analogy with known principle of Huyghens. Recall the manner of acoustic wave front construction according to the principle of Huyghens: at the moment $\mathbf{t}$ each front point is considered as a source of disturbances. The velocity of sound is the speed of propagation of a disturbance if gas is at rest. Taking into account flow velocity $\vec{\mathbf{W}}$, boundary of acoustic wave can be obtained as a boundary of disturbed medium.

Godunov method allows constructing the contour of contact discontinuity in the same manner. For that we use normal velocities of centers of each segment of the contact discontinuity obtained for the time step $\mathbf{t}$. Normal velocity $\mathbf{D}$ of each segment plays a similar role as speed of sound in the principle of Huyghens. Therefore construction of contact discontinuity segment at the time step $(t+\tau)$ begins with its normal transfer for a distance $\Delta = \tau\mathbf{D}$. But in contrast to the time step $\mathbf{t}$, at the time step $(t+\tau)$ two circles will be attached to the transferred segment of contact discontinuity. After that obtained construction at the time step $(t+\tau)$ has to be transferred for a vector $\tau \cdot \vec{\mathbf{W}}_{\mathbf{ss}}$. In the general case the magnitude of the vector $\tau \cdot \vec{\mathbf{W}}_{\mathbf{ss}}$ differs from zero.

Fig.2 demonstrates fulfillment of the algorithm. Here $\mathbf{L_1(t)}$, $\mathbf{L_2(t)}$ and $\mathbf{L_3(t)}$ are the segments of contact discontinuity at time step $\mathbf{t}$, $\mathbf{L_1(t+\tau)}$, $\mathbf{L_2(t+\tau)}$ and $\mathbf{L_3(t+\tau)}$ segments of contact discontinuity at time step $(t+\tau)$. Peculiarity of segments of contact discontinuity is that at time step $(t+\tau)$ circles are contiguous with the ends of segments. Dashed lines constructed as envelope achieved during propagation of disturbances for a distance $\tau\mathbf{D}$, and solid lines are obtained by the following transfer of the portions $\tilde{\mathbf{L}}_1(\mathbf{t}+\tau)$, $\tilde{\mathbf{L}}_2(\mathbf{t}+\tau)$ and $\tilde{\mathbf{L}}_3(\mathbf{t}+\tau)$ for corresponding vectors $\tau \cdot \vec{\mathbf{W}}_{\mathbf{ss}}$.

$\mathbf{P_1}$, $\mathbf{P_2}$ and $\mathbf{P_3}$ on Fig.2 are the guidelines. Guideline $\mathbf{P_2}$ intersects with $\mathbf{L_1(t+\tau)}$ in the point $\mathbf{T_2}$ and with $\mathbf{L_2(t+\tau)}$ in the point $\mathbf{N_2}$. Guideline $\mathbf{P_3}$ intersects with $\mathbf{L_2(t+\tau)}$ in the point $\mathbf{T_3}$ and with $\mathbf{L_3(t+\tau)}$ in the point $\mathbf{N_3}$. According to principle of Huyghens at time step $(t+\tau)$ the new node of contact discontinuity will located on the guideline $\mathbf{P_2}$ at the point $\mathbf{N_2}$, and on guideline $\mathbf{P_3}$ at the point $\mathbf{N_3}$. As an example, on fig.2 both of these points lie on the portions of circumferences $\mathbf{L_2(t+\tau)}$ and $\mathbf{L_3(t+\tau)}$ correspondingly. Also notice that previously the analogy with principle of Huyghens has been successfully used for

resolution of shock waves in the framework of Euler equations (Kraiko, A.N., et al., 1980, and Mileshin, V.I., 1986).

EXAMPLE OF SOLUTION OF A QUASI-3D INVERSE PROBLEM FOR NAVIER-STOKES EQUATIONS

As mentioned above, to solve inverse problem static pressure distribution has to be given along suction or pressure surface of blade. To prevent self-intersection of blade surface only suction surface (or pressure surface) is determined in the process of solution, coordinates of pressure surface (suction surface) are determined from given blade thickness. If static pressure distribution is such that there is no self-intersection of blade surface, then both suction and pressure surfaces are designed without regard for blade thickness.

An example is application of quasi-3D inverse Navier-Stokes-based solver to redesign rotor of high-loaded compressor stage (total pressure ratio $\boldsymbol{\pi^*_{stage}=1.7}$, theoretical work input coefficient $\boldsymbol{\bar{H}_T=0.384}$). Main peculiarity of the rotor is supersonic flow on suction surface with pre-shock Mach number equal to 1.3.

Suppression of shock-induced flow separation by decrease of maximum Mach number was the design target. To diminish pre-shock Mach number six blade sections on surfaces of revolution lying between 20% and 80% of blade height have been redesigned. Main aim was 0.1 drop of pre-shock Mach number. Performances of initial stage: $\pi^*_{rotor}=1.73$, $\eta^*_{ad\ rotor}=0.874$, $\pi^*_{stage}=1.70$, $\eta^*_{ad\ stage}=0.849$. Performances of inverse design: $\pi^*_{rotor}=1.72$, $\eta^*_{ad\ rotor}=0.892$, $\pi^*_{stage}=1.69$, $\eta^*_{ad\ stage}=0.867$. Guide vane of the stage remains the same in this investigation.

Fig.3 demonstrates Mach number level lines on suction surface of initial (left) rotor blade and redesign (right). It shows that 0.1 diminishing of pre-shock Mach number makes Mach level lines aft-shifted. Besides that, separation zone located at 75% of initial blade height is fully eliminated in re-designed blade flow.

Fig.4 demonstrates Mach level lines for initial airfoil (left) and redesign (right) of blade section located at 50% of blade height.

Comparison of radial distributions of adiabatic efficiency at the outlet of initial rotor and redesign is shown on fig.5. Within redesign range (from 20% to 80% of blade height) adiabatic efficiency increases. Fig.6 explains that adiabatic efficiency increase has been achieved by diminishing of total temperature growth accompanied by maintained total pressure ratio.

Fig7. presents static pressure distributions for three sections of initial blade and redesign of the rotor.

CONCLUSIONS

New quasi-3D inverse non-iterative redesign method for a stationary or rotating cascade of axial compressor blade row is presented. Main advantage of the method is application to viscous flow, i.e. airfoil is shaped by integration of Navier-Stokes equations from given static pressure distribution along airfoil contour. Another advantage is that this approach to solution of inverse problem can be extended to 3D flows. Being combined with 3D viscous Navier-Stokes solver this method is a useful tool for design of a multi-stage axial compressor.

Inverse redesign method presented in this paper has been applied to improve adiabatic efficiency of a high-loaded rotor of axial compressor stage. Suppression of shock-induced flow separation by decrease of maximum Mach number as a design target has been successfully achieved.

REFERENCES

Dang, T., Damie, S., and Qiu, X., 2000, "Euler-Based Inverse Method for Turbomachine Blades. Part 2: Three-Dimensional Flows," AIAA Journal, Vol. 38, №11, pp. 2007-2013.

Demeulenaere, A., and Leonard, and Van den Braembussche, R.A., 1997, "A Two-Dimensional Navier-Stokes Inverse Solver for Compressor and Turbine Blade Design", Procedings of the Second European Conference on "Turbomachinery - Fluid Dynamics and Thermodynamics", Antwerp, Belgium, 339-346.

Demeulenaere, A, and Van den Braembussche, R.A., 1996, "Three-Dimensional Inverse Method for Turbomachinery Blading Design," ASME Journal of Turbomachinery, 120(1), 247-255.

De Vito, L., Van den Braembussche, R.A., and Deconinck, H., 2002, "A Novel Two Dimensional Viscous Inverse Design Method for Turbomachinery Blading", Proceedings of ASME TURBO EXPO 2002, June 3-6, Amsterdam, The Netherlands, GT-2002-30617, pp. 1-10.

Godunov, S.K., Zabrodin, A.V., Ivanov, M.Ya., Kraiko, A.N., Prokopov, G.P., 1976, "Numerical Solution of Multi-Dimensional Problems of Gas Dynamics", M.: "Nauka", (in Russian).

Gouskov, O.V., Kopchenov, V.I., Nikiforov, D.A., 1994, "Flow numerical simulation in the propulsion elements of aviation space system within full Navier-Stokes equations", In International Conference on the Methods of Aerophysical Research, Proceedings, Part 1, Novosibirsk, p. 104-109.

Ivanov, M.Ya., Krupa, V.G., Nigmatullin, R.Z., 1989, "Implicit S.K.Godunov's scheme of Raised Accuracy for Integration of Navier-Stokes Equations ", Journal of Computational Mathematics and Mathematical Physics, v.29, pp. 888-901 (in Russian).

Kraiko, A.N., Makarov, V.E., Tillyaeva, N.I., 1980, "To Numerical Construction of Shock Wave Fronts", Journal of Computational Mathematics and Mathematical Physics, v.20, №3, pp. 716-723 (in Russian).

Meauze, G., 1982, "An Inverse Time Marching Method for the Definition of Cascade Geometry," Journal of Turbomachinery, Vol. 11, pp. 650-656.

Mileshin, V.I., 1986, "Computation of 3D Supersonic Flow within Engine Inlet at the Detached Shock Flow Regime", Journal of Computational Mathematics and Mathematical Physics, v.26, №11, pp. 1704-1718 (in Russian).

Mileshin, V.I., Startsev, A.N., Orekhov, I.K., 2000, "Method of design and development of axial and centrifugal compressors, based on 3D viscous flow analysis in the context of Navier-Stokes equations and solutions ofquasi-3D inverse problems of gasdynamics", Vol.2, "Scientific contribution to design of aviation engines," Ed. V.A. Skibin and V.I. Solonin, Moscow, Macihe building, (in Russian).

Mileshin, V.I., Startsev, A.N., Orekhov, I.K., Pankov, S.V., 2001, "Computational and Experimental Investigation of High Pressure Axial and Centrifugal Compressors with Ultra-High Rotational Speed," XV International Symposium on Airbreathing Engines, Bangalore, India, September 2-7, ISABE 2001-1115.

Mileshin, V.I., Zhuravlev, V.V., Kraiko, A.N., Startsev, A.N., Orekhov, I.K., Schipin, S.K., 1992, "Calcul Transsoniques et Supersoniques Tri- et Quasi-Tridimensionnels pour Compresseurs Axial et Centrifugees", J. Mechanique de France, №1992-4.

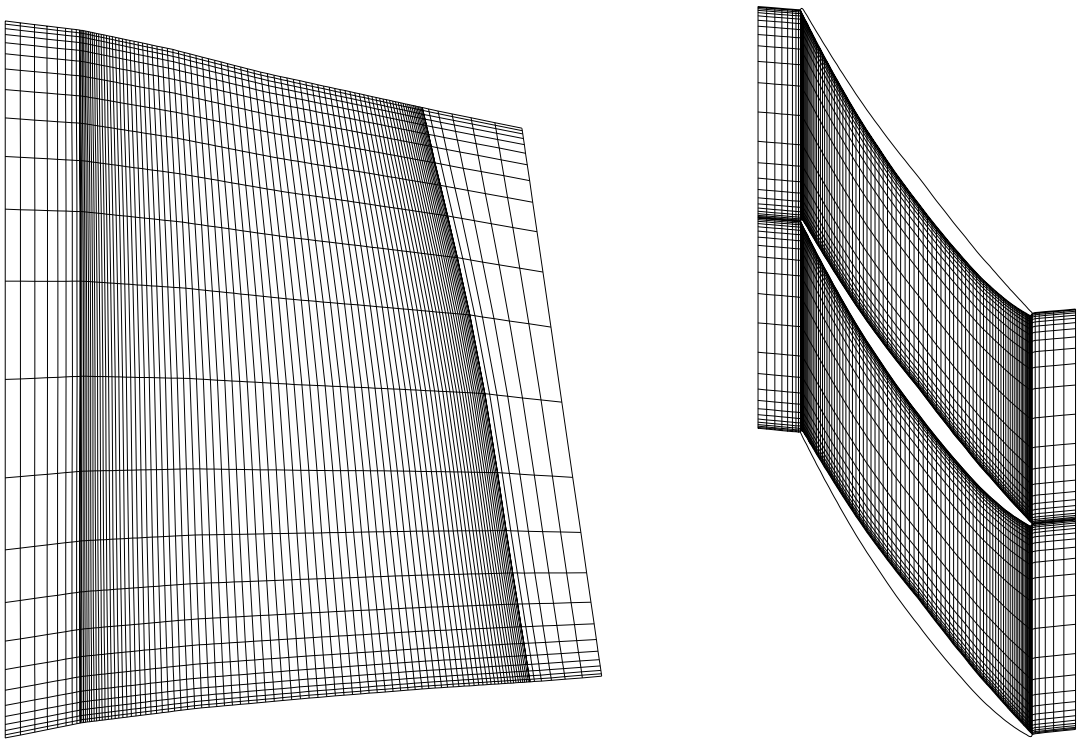

Fig.1 Grid

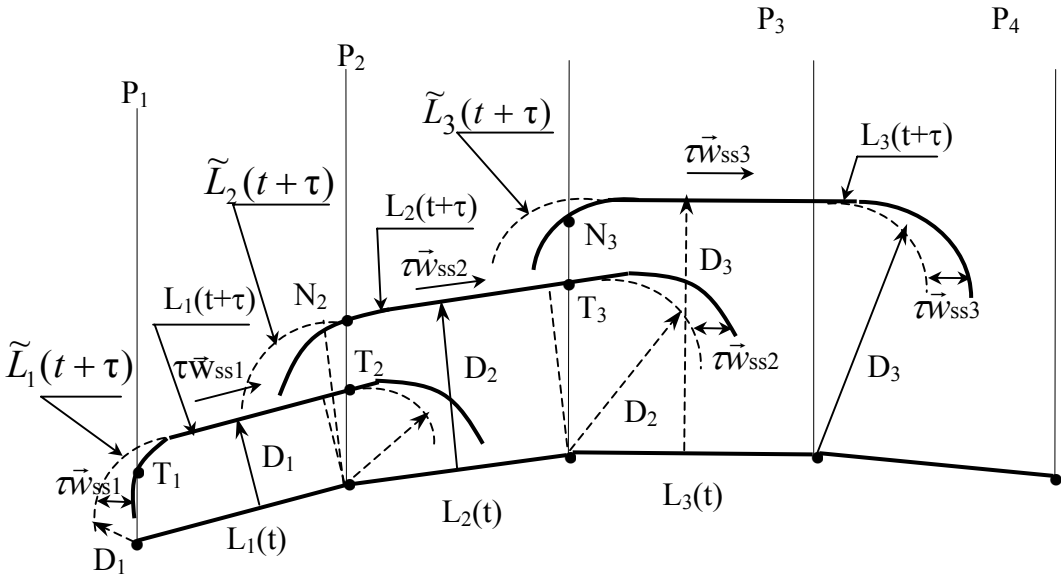

Fig. 2

Initial rotor **Inverse design**

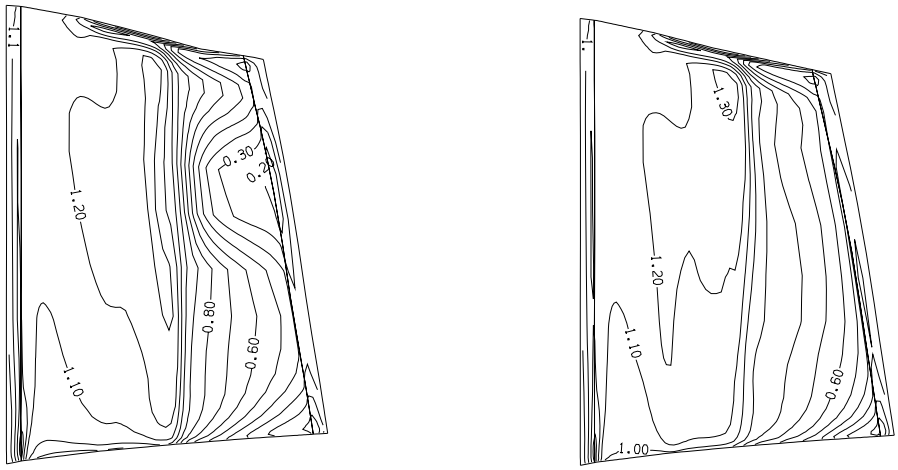

Fig. 3 Rotor of high-pressure compressor. Suction side of blade. Mach number level lines, step = 0.1 Left – initial design, right – inverse design. Performances of initial design: π^*_{rotor} =1.73 $\eta^*_{ad\ rotor}$ = 0.874 π^*_{stage} = 1.70 $\eta^*_{ad\ stage}$ = 0.849. Performances of inverse design: π^*_{rotor} =1.72 $\eta^*_{ad\ rotor}$ = 0.892 π^*_{stage} = 1.69 $\eta^*_{ad\ stage}$ = 0.867.

Initial rotor **Inverse design**

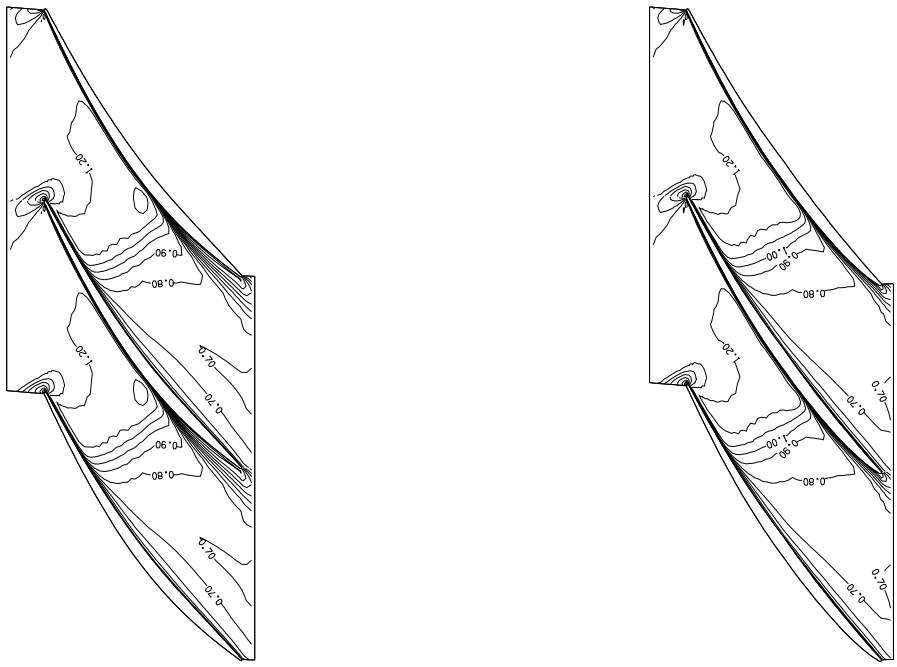

Fig. 4 Rotor of high-pressure compressor. 50% of blade height. Mach number level lines, step = 0.1 Left – initial design, right – inverse design. Performances of initial design: π^*_{rotor} =1.73 $\eta^*_{ad\ rotor}$ = 0.874 π^*_{stage} = 1.70 $\eta^*_{ad\ stage}$ = 0.849. Performances of inverse design: π^*_{rotor} =1.72 $\eta^*_{ad\ rotor}$ = 0.892 π^*_{stage} = 1.69 $\eta^*_{ad\ stage}$ = 0.867.

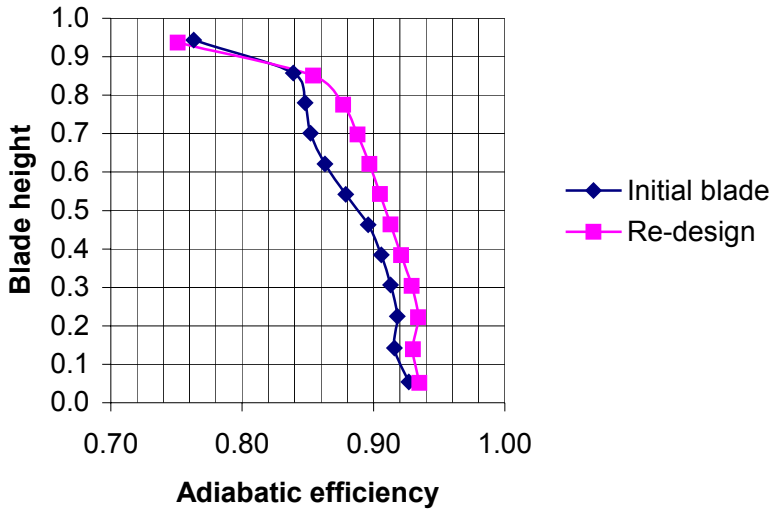

Fig. 5 Radial distribution of rotor's adiabatic efficiency. Comparison of initial design (diamonds) and redesign (squares). Performances of initial design: $\pi^*_{rotor} = 1.73$ $\eta^*_{ad\ rotor} = 0.874$ $\pi^*_{stage} = 1.70$ $\eta^*_{ad\ stage} = 0.849$. Performances of inverse design: $\pi^*_{rotor} = 1.72$ $\eta^*_{ad\ rotor} = 0.892$ $\pi^*_{stage} = 1.69$ $\eta^*_{ad\ stage} = 0.867$

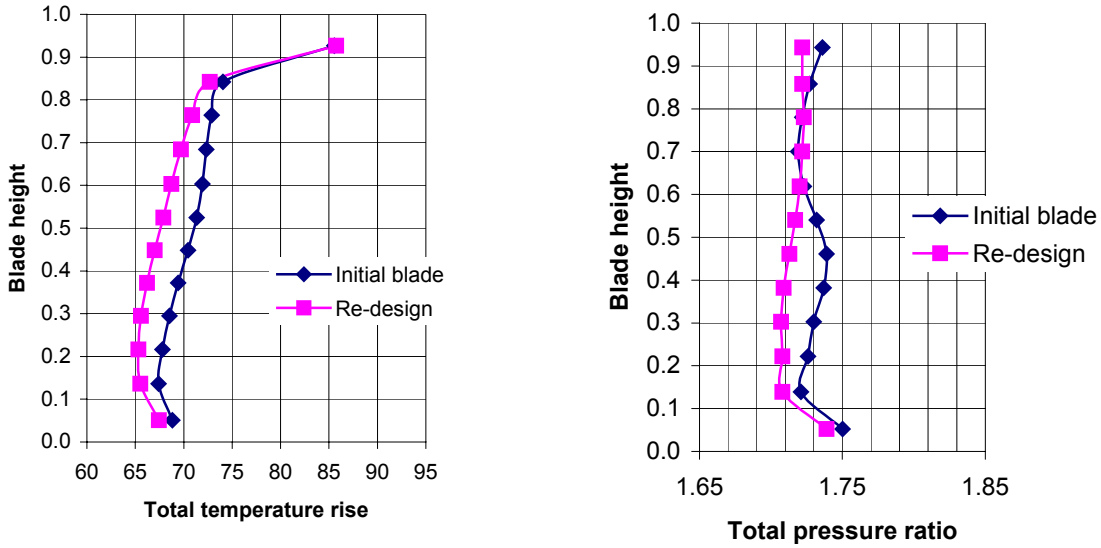

Fig. 6 Radial distribution of rotor's total temperature rise (left) and total pressure ratio (right) at the exit of rotor. Comparison of initial design (diamonds) and redesign (squares).

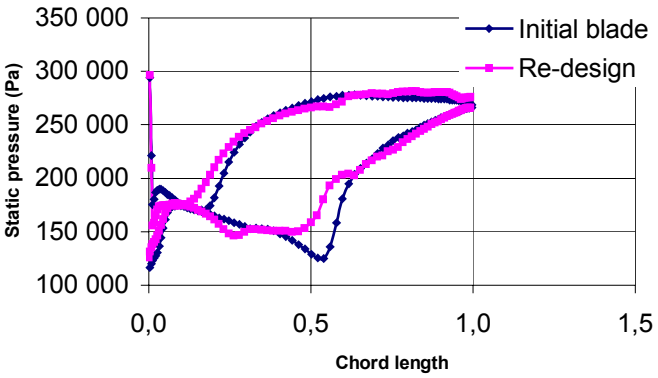

a)

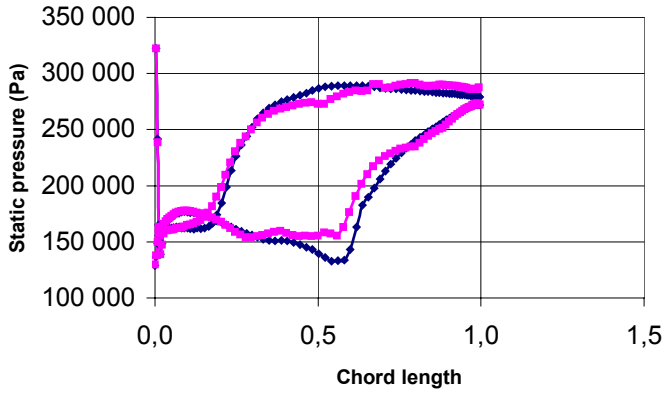

b)

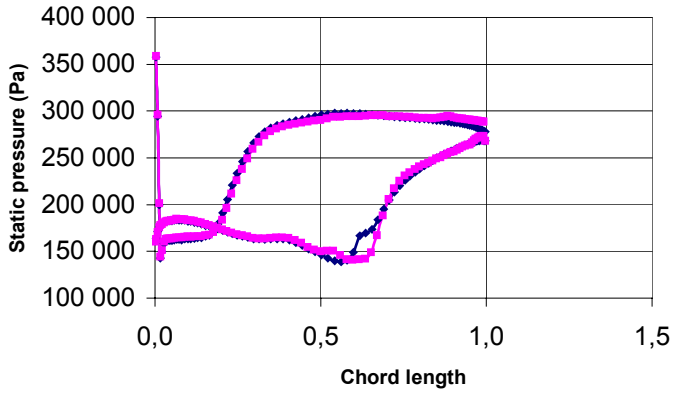

c)

Fig.7 Static pressure distributions on hub (20% of blade height) – a), mid-span (50% of blade height) – b), and tip (80% of blade height) –c) of initial and re-designed rotor. Static pressure distributions are resulted from 3D viscous flow calculation of axial compressor as a whole.